

Radiolabeled $\alpha_v\beta_3$ Integrin Antagonists: A New Class of Tracers for Tumor Targeting

Roland Haubner, Hans-Jürgen Wester, Ute Reuning, Reingard Senekowitsch-Schmidtke, Beate Diefenbach, Horst Kessler, Gerhard Stöcklin and Markus Schwaiger

Department of Nuclear Medicine, Women's Hospital, Clinical Research Unit and Institute of Organic Chemistry and Biochemistry, Technische Universität München, Munich; and Merck KGaA, Darmstadt, Germany

The $\alpha_v\beta_3$ integrins play an important role during tumor metastasis and tumor-induced angiogenesis. Targeting of this receptor may provide information about the receptor status of the tumor and enable specific therapeutic planning. Cyclo(-Arg-Gly-Asp-D-Phe-Val-) has been shown to be a selective $\alpha_v\beta_3$ integrin antagonist with high affinity. In this study we describe the synthesis and biological evaluation of [125 I]-3-iodo-D-Tyr⁴-cyclo(-Arg-Gly-Asp-D-Tyr-Val-) ([125 I]P2), [125 I]-3-iodo-Tyr⁶-cyclo(-Arg-Gly-Asp-D-Phe-Tyr-) ([125 I]P4) and the negative control peptide [125 I]-3-iodo-D-Tyr⁴-cyclo(-Arg-D-Ala-Asp-Tyr-Val-) ([125 I]P6). **Methods:** Peptides were assembled on a solid support using fluorenylmethoxycarbonyl amino acid coupling protocols. Radioiodination was performed using the iodogen method. The in vitro binding assays were performed using isolated, immobilized $\alpha_{IIB}\beta_3$ and $\alpha_v\beta_3$ integrins. Expression of the $\alpha_v\beta_3$ receptor on the different tumors was validated by immunohistochemical methods using α_v and $\alpha_v\beta_3$ specific antibodies. For biodistribution studies, nude mice with melanoma M21 or mammary carcinoma MaCaF and BALB/c mice with osteosarcoma were used. **Results:** The in vitro binding assays demonstrate that the introduction of tyrosine and subsequent iodination have no influence on the high affinity and selectivity for $\alpha_v\beta_3$. Immunohistochemical staining clearly indicates the presence of the $\alpha_v\beta_3$ integrins on the tumor tissue of the melanoma and the osteosarcoma. Pretreatment and displacement studies show specific binding of [125 I]P2 on melanoma M21-bearing nude mice and osteosarcoma-bearing BALB/c mice but less specific binding on mammary carcinomas. [125 I]P2 exhibits fast elimination kinetics. The accumulation in the tumor 10 min postinjection is 2.07 ± 0.32 %ID/g for the melanoma M21 and 3.50 ± 0.49 %ID/g for the osteosarcoma and decreases to 1.30 ± 0.13 %ID/g and 2.03 ± 0.49 %ID/g 60 min postinjection, respectively. [125 I]P4 shows even faster elimination kinetics, resulting in a tumor accumulation of 0.40 ± 0.10 %ID/g 60 min postinjection for the osteosarcoma-bearing BALB/c mice. Both peptides reveal predominately hepatobiliary excretion. For [125 I]P2, this also is confirmed by autoradiography. The negative control peptide [125 I]P6 shows no specific activity accumulation. **Conclusion:** [125 I]P2 exhibits high affinity and selectivity for the $\alpha_v\beta_3$ integrin in vitro and in vivo and, thus, represents the first radiolabeled $\alpha_v\beta_3$ antagonist for the investigation of angiogenesis and metastasis in vivo.

Key Words: RGD peptides; alpha(v)beta(3) antagonists; integrins; 125 I labeling; tumor targeting

J Nucl Med 1999; 40:1061-1071

Radiolabeled derivatives of regulatory peptides, such as the vasoactive intestinal peptide and especially somatostatin, are used for tumor targeting (1). However, not all neoplasms express the corresponding receptors. Therefore, it is mandatory to search for additional receptors that are overexpressed on tumor cells. Members of the cell adhesion receptor families could be promising candidates.

Cell-cell and cell-matrix interactions play an important role in tumor metastasis (2,3). These interactions are essential during dissociation of individual cells from the primary tumor and invasion of the adjacent tissue, for adherence in the capillary bed of the target organ and during extravasation and arrest in the foreign tissue (Fig. 1). One cell surface receptor class participating in these cell adhesion processes is the integrins (2-4). They are heterodimeric, transmembrane glycoproteins consisting of an α - and a β -subunit (5,6). The most interesting members of this family are the glycoprotein IIb/IIIa ($\alpha_{IIB}\beta_3$), involved in platelet aggregation (5,7), and the vitronectin receptor $\alpha_v\beta_3$.

The $\alpha_v\beta_3$ integrin is implicated in many pathological processes, such as osteoporosis (8), misregulated angiogenesis (9) (e.g., rheumatoid arthritis or retinopathy) as well as tumor growth (10,11) and tumor metastasis (12,13). This receptor is highly expressed on many tumor cells (14,15), such as osteosarcomas, neuroblastomas, carcinomas of the lung, the breast, the prostate and the bladder, as well as glioblastomas (16) and invasive melanomas (12). Several investigations have shown a correlation between the expression of $\alpha_v\beta_3$ and the metastatic potential of melanomas (12,13,17) and gastric carcinomas (18). In addition, it has been shown that the $\alpha_v\beta_3$ integrin is also important during tumor-induced angiogenesis (9,10). The involved endothelial cells express $\alpha_v\beta_3$ to adhere on the extracellular matrix during migration toward the tumor (Fig. 1). In the chick chorioallantoic membrane model, inhibition of the $\alpha_v\beta_3$ integrin with monoclonal antibodies or peptidic antagonists

Received Apr. 30, 1998; revision accepted Oct. 20, 1998.

For correspondence or reprints contact: Roland Haubner, PhD, Department of Nuclear Medicine, Klinikum rechts der Isar, Technische Universität München, Ismaninger Str. 22, D-81675 München, Germany.

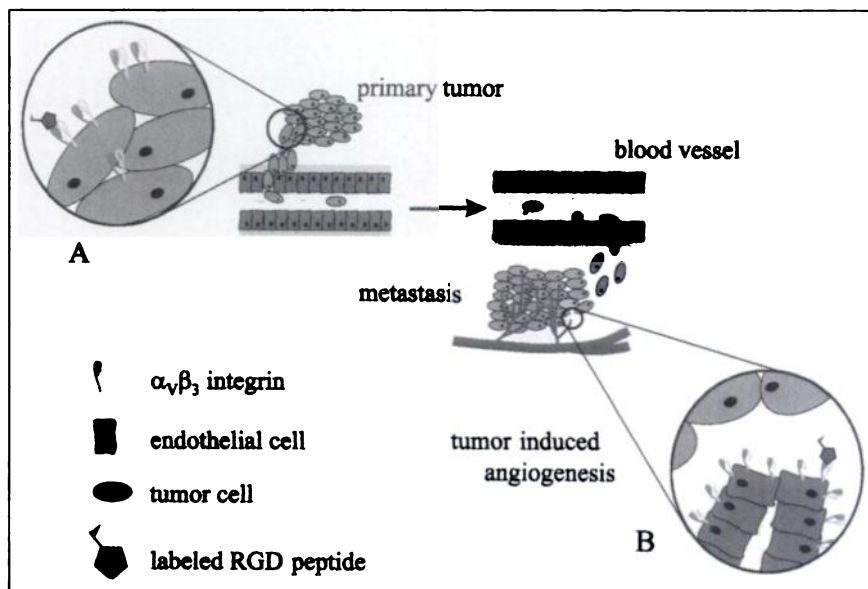


FIGURE 1. Targets for tumor imaging based on $\alpha_v\beta_3$ tracers (labeled RGD peptides). $\alpha_v\beta_3$ integrins are highly expressed on metastatic tumors (A) and on endothelial cells undergoing angiogenesis (B).

results in a drastic reduction of neovascularization around the tumor, leading to the starvation of the tumor.

Several investigators are searching for selective $\alpha_v\beta_3$ antagonists with high affinity for therapeutic use (19). However, for successful therapy, the determination of the $\alpha_v\beta_3$ receptor status on the tumor cells and the surrounding endothelial cells of the spreading blood vessels is important. The development of radiolabeled $\alpha_v\beta_3$ antagonists, in combination with PET, should allow targeting of $\alpha_v\beta_3$ positive tumors (tumor cells or involved endothelial cells) and an *in vivo* quantification of the receptor density and, thus, provide a helpful tool for therapeutic planning. In addition, these tracers should permit *in vivo* control of the therapeutic successes.

In this study, we describe the synthesis and characterization of the ^{125}I -labeled peptidic $\alpha_v\beta_3$ antagonists and their biological evaluation *in vitro* and *in vivo*.

The integrins bind to a wide variety of extracellular matrix proteins (5). A common receptor recognition motif of

these matrix proteins is the peptide sequence Arg-Gly-Asp (single letter coding: RGD) (20). These findings gave rise to the search for small RGD-containing integrin antagonists (19). Our first investigations of the RGD peptides led to the selective $\alpha_v\beta_3$ antagonist cyclo(-Arg-Gly-Asp-D-Phe-Val-) with IC_{50} values in the lower nanomolar range (21–23). Additional results showed that, besides the essential RGD sequence, a hydrophobic amino acid in position 4 increases the affinity, whereas the amino acid in position 5 has no influence on the affinity (24).

These studies provide a peptide that can be modified for use as a radioactive tracer in PET and SPECT (Fig. 2). On the one hand, substitution of the amino acid in position 4 (D-Phe in lead structure) or 5 (Val in lead structure) with tyrosine allows electrophilic radiohalogenation (e.g., ^{125}I , ^{131}I). On the other hand, replacement of the amino acid in position 5 with lysine offers a further alternative for radiolabeling by prosthetic groups (e.g., ^{18}F , ^{123}I) or conjugation with chelators for metal isotopes (e.g., $^{99\text{m}}\text{Tc}$, ^{111}In)

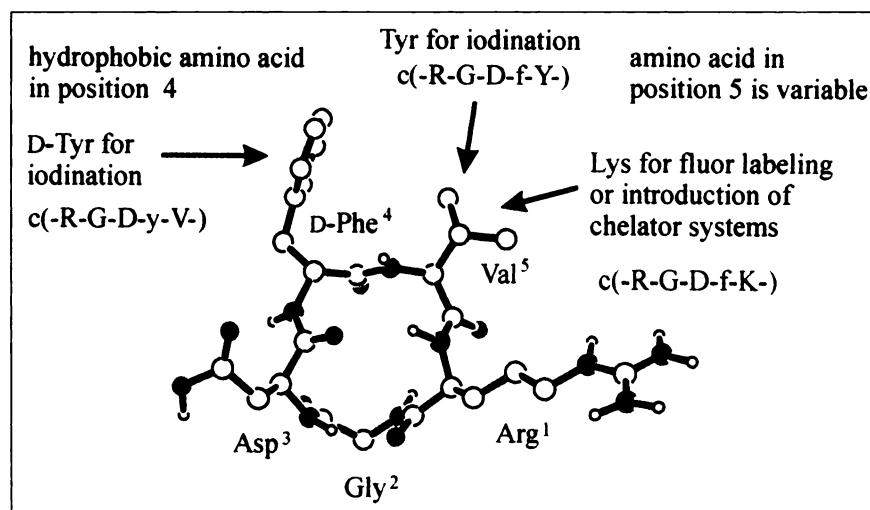


FIGURE 2. Structure of cyclo(-Arg-Gly-Asp-D-Phe-Val-). Possible targets for modification are amino acids in positions 4 and 5. For first biodistribution experiments, D-Phe⁴ as well as Val⁵ are substituted with tyrosine, resulting in cyclo(-Arg-Gly-Asp-D-Tyr-Val-) (P1) and cyclo(-Arg-Gly-Asp-D-Phe-Tyr-) (P3), respectively. Large open circles = carbon; small open circles = hydrogen; dark gray circles = nitrogen; light gray circles = oxygen.

(25,26). For the first biodistribution studies, we chose the two radioiodinated tyrosine derivatives [¹²⁵I]-3-iodo-D-Tyr⁴-cyclo(-Arg-Gly-Asp-D-Tyr-Val-) ([¹²⁵I]P2) and [¹²⁵I]-3-iodo-Tyr⁵-cyclo(-Arg-Gly-Asp-D-Phe-Tyr-) ([¹²⁵I]P4). Pretreatment and displacement experiments were performed using cyclo(-Arg-Gly-Asp-D-Phe-Val-), which reveals high affinity for the $\alpha_v\beta_3$ integrin. The extent of nonspecific binding was quantified with the radioiodinated negative control peptide [¹²⁵I]-3-iodo-Tyr⁴-cyclo(-Arg-D-Ala-Asp-Tyr-Val-) ([¹²⁵I]P6).

MATERIALS AND METHODS

All chemicals were used as supplied without further purification. Except for N-methylpyrrolidone (NMP), all organic solvents were distilled before use. The 9-fluorenylmethoxycarbonyl (Fmoc) amino acids were purchased from Bachem (Heidelberg, Germany), Novabiochem (Bad Soden, Germany) and Alexis (Grünberg, Germany). The tritylchloride polystyrol (TCP) resin was purchased from PepChem (Tübingen, Germany). The 1-hydroxybenzotriazol (HOBt) was synthesized using the method described by König and Geiger (27). O-(1H-benzo-triazol-1-yl)-N,N,N',N'-tetramethyluronium tetrafluoroborate (TBTU) and diphenyl phosphorazidate (DPPA) were purchased from Alexis and Aldrich (Steinheim, Germany), respectively. Sodium iodide-125 was purchased from Amersham (Buckinghamshire, UK). All other organic reagents were purchased from Merck (Darmstadt, Germany), Aldrich or Fluka (Neu-Ulm, Germany).

Mass spectra were recorded on the LC-MS system LCQ from Finnigan (Bremen, Germany) using the Hewlett Packard series 1100 HPLC system. NMR-spectra were recorded on a Bruker AC 250 (Karlsruhe, Germany) at 300 K. For all experiments, the solvent signal was used for calibration.

Analytic reversed-phase high-performance liquid chromatography (RP-HPLC) was performed on Beckmann (München, Germany) or Sykam equipment (Gilching, Germany), using columns with YMC-Pack ODS-A (5 μ m, 250 \times 4 mm) or LiChrospher 100 RP 18 (7 μ m, 250 \times 4 mm). For radioactivity measurements, the outlet of the ultraviolet detector was connected to a well type NaI(Tl) detector from EG&G (München, Germany). For analytic data, several acetonitrile/water gradients with 0.1% trifluoroacetic acid (TFA) were used.

Preparative RP-HPLC was performed with the Sykam HPLC system or the Beckman System. Columns were YMC-Pack ODS-A (5 μ m, 250 \times 30 mm) or Macherey-Nagel Nucleosil C-18 (7 μ m, 250 \times 40 mm) for peptides P1, P3 and P5 and LiChrospher 100 RP 18 (7 μ m, 250 \times 4 mm) for [¹²⁵I]P2, [¹²⁵I]P4 and [¹²⁵I]P6 with the same solvent system as above.

Synthesis of Fmoc-3-iodo-Tyr-OH and Fmoc-3-iodo-D-Tyr-OH

Iodination of Tyrosine. First, 6.4 g (52 mmol) iodine in 50 mL ethanol were added slowly to a solution of 4.7 g (26 mmol) tyrosine (D- or L-configuration) in 500 mL 25% aqueous ammonia and stirred continuously. After 1 h, the solution was concentrated in vacuo until precipitation started. Crystallization was accomplished overnight at 4°C. The crude product was aspirated and recrystallized from a small amount of water: yield 2.9 g (36.1%); HPLC: t_R = 18.2 min; K' = 7.3 (5%–50% acetonitrile [MeCN]; 30 min); ¹H-NMR (D₂O) δ 2.97 ppm (dd, 1H, 7.6 Hz, 14.7 Hz), 3.09 ppm

(dd, 1H, 5.7 Hz, 14.7 Hz), 4.12 ppm (dd, 1H, 5.8 Hz, 7.6 Hz), 6.77 ppm (d, 1H, 8.4 Hz), 7.02 ppm (dd, 1H, 2.2 Hz, 8.4 Hz), 7.54 ppm (d, 1H, 2.2 Hz).

N-terminal Protection with Fmoc-Cl. N-terminal protection followed the synthesis described by Chang et al. (28). Briefly, 6.9 mmol 3-iodo-tyrosine were dissolved in 10 mL 10% sodium bicarbonate and 5 mL dioxane at 0°C. Fmoc-Cl (6.9 mmol) in 7 mL dioxane was added, and the solution was stirred for 1 h at 0°C and further stirred overnight at ambient temperature. The reaction mixture was poured into ice water and extracted with ethyl ether. The aqueous layer was acidified with hydrochloric acid to pH 2 and extracted with ethyl ether. The combined organic layers were washed with 0.1 N HCl solution and water, dried with MgSO₄ and evaporated to dryness under reduced pressure: yield 3 g (81.9%) (95% pure according to HPLC); HPLC: t_R = 24.0 min; K' = 9.9 (30%–80% MeCN; 30 min); ¹H-NMR (DMSO-d₆) δ 2.72 ppm (dd, 1H), 2.94 ppm (dd, 1H), 4.10 ppm (m, 1H), 4.20 ppm (m, 3H), 6.78 ppm (d, 1H), 7.10 ppm (dd, 1H), 7.24–7.46 ppm (m, 4H), 7.57–7.74 ppm (m, 4H), 7.90 ppm (d, 2H), 10.11 ppm (s, 1H).

Synthesis of the Cyclic Pentapeptides

Loading of the TCP Resin. Fmoc-Gly-OH or Fmoc-D-Ala-OH (1.3 mmol) was dissolved in 7 mL dry dichloromethane (DCM) and 190 μ L (1.1 mmol) diisopropylethylamine (DIEA). The solution was added to 1.0 g resin (1 mmol Cl⁻/g resin) in a flask. After 5 min, an additional 380 μ L (2.2 mmol) DIEA were added, and the reaction mixture was stirred for 1 h at ambient temperature. Finally, 1 mL methanol was added, and the mixture was allowed to further react for 20 min. The solution was removed, and the resin was washed twice with DCM and dimethylformamide (DMF), followed by mixtures of DMF/methanol, successively increasing the methanol content up to pure methanol under rapid stirring.

Peptide Synthesis. Starting with 1.0–2.0 g Fmoc-Gly-TCP or Fmoc-D-Ala-TCP resin (substitution about 0.4–0.6 mmol amino acid/g resin), synthesis was performed using standard Fmoc coupling protocols. Deprotection of the N-terminal Fmoc group was accomplished using 20% piperidine in DMF. Coupling of the amino acids or amino acid derivative was performed using 2.5 equiv. of the appropriate amino acid, 2.5 equiv. TBTU, 2.5 equiv. HOBt and 5–7.5 equiv. DIEA in 20 mL NMP. Coupling times between 30 and 60 min provided complete couplings. The reactions were monitored by ninhydrine test. Side chain protection was 4-methoxy-2,3,6-trimethylbenzenesulfonyl for arginine and tert-butyl for aspartic acid and tyrosine.

Acetic Acid Cleavage. The resin-bound peptides were treated with 20 mL of a mixture of acetic acid, 2,2,2-trifluoroethanol (TFE) and DCM (3:1:6) for 2 h at ambient temperature. The resin was washed twice with 20 mL of a mixture of acetic acid, TFE and DCM (3:1:6). The combined solution was evaporated in vacuo in the presence of toluene and triturated with ethyl ether, filtered and washed three times with ethyl ether.

Cyclization. The peptides were dissolved in DMF (concentration 5×10^{-3} mol/L). Five equiv. NaHCO₃ and 3 equiv. DPPA were added (for 3-iodo-tyrosine containing peptides, 1 equiv. DPPA was used), and the solution was stirred at ambient temperature for 24 h. After filtration of the solid NaHCO₃, DMF was evaporated in vacuo, and the residue was triturated with water, filtered and washed with water and ethyl ether.

Side Chain Deprotection and Purification. The cyclic peptides were treated with 20 mL of a solution of 95% TFA, 2.5% water and

2.5% ethane dithiol for 24 h at ambient temperature. The mixture was filtered (if necessary), evaporated in vacuo, triturated with ethyl ether, filtered and washed several times with ethyl ether. The crude, cyclic peptides were purified by RP-HPLC. Analytic data are given in Table 1.

Radiiodination

The peptides P1, P3 and P5 were labeled with ^{125}I using the iodogen method. The peptides (0.8 μmol) were dissolved in 300 μL phosphate buffered saline (PBS), pH 7.4 (8.00 g/L NaCl, 0.20 g/L KCl, 0.20 g/L KH_2PO_4 , 1.44 g/L $\text{Na}_2\text{HPO}_4 \times 2\text{H}_2\text{O}$). The solutions were added to Eppendorf caps coated with 150 μg iodogen and combined with 5–10 μL n.c.a. [^{125}I]NaI (30–60 MBq). After 30 min at ambient temperature, the solutions were removed from the solid oxidizing reagent. Purification was performed using RP-HPLC. Radiochemical purity was generally >95%. After removing the solvent in vacuo, the residue was triturated with water, passed through a C_{18} Sep-Pak column, washed two times with water (2 mL) and eluted with 2 mL methanol. The methanol was removed in vacuo, and the residue was dissolved with PBS pH 7.4 to obtain solutions with an activity concentration of 370 kBq (10 μCi)/100 μL that were ready for use in animal experiments. The specific activity was between 41 and 56 TBq (1100 and 1500 Ci)/mmol, and the overall radiochemical yield after RP-HPLC was about 50%.

Biological Assay

Protein Purification. Human plasma vitronectin (29) and fibrinogen (30) were purified as described previously. The $\alpha_v\beta_3$ integrin was purified from human placenta (31) with modifications (32). Briefly, human placenta was extracted with octyl- β -D-glucopyranoside at 4°C. The extract was cleared by centrifugation circulated over an LM609 antibody column (33), and specifically bound material was eluted at pH 3.1. The eluant was neutralized, dialyzed against NP-40 (0.1% in PBS pH 7.4), concentrated to >1 mg/mL and stored at -70°C .

The $\alpha_{\text{IIb}}\beta_3$ integrin was prepared from human platelets (34) with modifications (32). Briefly, platelets were extracted with octyl- β -D-glucopyranoside (50 mmol/L). The extract was circulated over a linear Gly-Arg-Gly-Asp-Ser-Pro-Lys-conjugated CL-4B Sepharose column, and specifically bound material was eluted with linear peptide Gly-Arg-Gly-Asp-Ser-Pro-Lys. The eluant was dialyzed

against NP-40 (0.1% in PBS pH 7.4), concentrated to >1 mg/mL and stored at -70°C .

Both preparations were ~95% pure as judged by anti-integrin enzyme-linked immunosorbent assay (ELISA) using α - and β -chain specific monoclonal antibodies and by sodium dodecyl sulfate polyacrylamide gel electrophoresis.

Isolated Integrin Binding Assays. Inhibitory effects of cyclic peptides were quantified by measuring their effects on the interactions between immobilized integrin and biotinylated soluble ligands. Purified vitronectin or fibrinogen (1 mg/mL; pH 8.2) were biotinylated with N-hydroxysuccinimide biotin (100 $\mu\text{g}/\text{mL}$; 1 h, 20°C), before dialysis into PBS pH 7.4. Purified integrin (1 $\mu\text{g}/\text{mL}$; 1 h, 4°C) was used to coat 96-well microtitre plates, which were then blocked with bovine serum albumin (BSA) (3% in 1 mmol/L CaCl_2 , 1 mmol/L MgCl_2 , 10 $\mu\text{mol}/\text{L}$ MnCl_2 , 100 mmol/L NaCl, 50 mmol/L tris(hydroxymethyl)-aminomethane; pH 7.4), and incubated (3 h at 30°C) with biotinylated ligands (1 $\mu\text{g}/\text{mL}$ in binding buffer: 0.1% BSA, 1 mmol/L CaCl_2 , 1 mmol/L MgCl_2 , 10 $\mu\text{mol}/\text{L}$ MnCl_2 , 100 mmol/L NaCl, 50 mmol/L tris(hydroxymethyl)-aminomethane; pH 7.4) in the presence or absence of serially diluted peptides. After washing (3×5 min with binding buffer), bound biotinylated ligand was detected with alkaline-phosphatase conjugated goat-antibiotin antibodies (1 $\mu\text{g}/\text{mL}$; 1 h, 37°C), using p-nitrophenyl phosphate as chromogen. Vitronectin binding in the absence of competitor was defined as 100% signal; binding to blocked wells in the absence of integrin was defined as 0%. Signal-to-noise ratio was >10. Concentrations of peptides required for 50% inhibition of signal (IC_{50} values) were estimated graphically. Assays were performed in triplicate. The linear heptapeptide Gly-Arg-Gly-Asp-Ser-Pro-Lys was included as external reference, and IC_{50} values were normalized to the reference IC_{50} to give a value Q, which allowed comparison of IC_{50} between different experiments.

In Vivo Animal Experiments

Tumor Xenografts. Human tumor xenografts were established in athymic mice by subcutaneous inoculation with 1 mm^3 primary tissue from patients with solid ductal mammary carcinoma (MaCaF) (35). Tumors grown to a weight of approximately 500 mg were used for further propagation in nude mice. Every passage was checked by immunohistochemical staining, using an anti-mouse IgG antibody and an anti-human IgG antibody, to confirm that the implanted tumor tissue was still of human origin and comparable with the primary tissue.

Osteosarcomas induced by injection of ^{90}Sr were serially transplanted into BALB/c mice. Tumor pieces of 1 mm^3 were injected by trocar close to the femur into the musculus quadriceps. Mice with tumor weights of about 500 mg were chosen for further investigations.

Tumors derived from the human M21 melanoma cell line (33) were obtained by subcutaneous injection of 5×10^6 cells. Cells were grown routinely in a monolayer culture at 37°C in a 5% CO_2 humidified air atmosphere. Mice with tumors weighing 300–400 mg were chosen for biodistribution and tumor-uptake studies.

Biodistribution Studies. Nude mice bearing tumor xenografts of human melanoma M21 or mammary carcinoma (MaCaF), and BALB/c mice bearing osteosarcoma, were injected intravenously with 10 μCi [^{125}I]P2, [^{125}I]P4 or the negative control peptide [^{125}I]P6 in groups of two to five for every substance and assay time.

The animals were killed and dissected 10, 60, 120 and 240 min after injection of the ^{125}I -labeled peptides. Tumor, blood, plasma, muscle, liver, kidney and thyroid were removed and weighed. The

TABLE 1
Analytic Data of Cyclic Peptides HPLC: 5 Minutes
10% MeCN/0.1% Trifluoroacetic Acid (TFA);
10%–50% MeCN/0.1% TFA in 30 Minutes

Number	Peptide	Mol wt (g/mol)	ESI-MS (M + H) ⁺	t _R (min)	K'
P1	c(RGDyV)	590.64	591	13.0	4.9
P2	c(RGD(I)yV)	716.53	717	21.2	8.6
P3	c(RGDFY)	638.68	639	19.1	7.7
P4	c(RGDf(I)Y)	764.58	765	24.7	10.2
P5	c(RaDYV)	604.66	605	16.9	6.7

HPLC = high-performance liquid chromatography; ESI-MS = electrospray ionization mass spectroscopy; t_R = retention time; K' = capacity factor.

radioactivity in the tissue was measured using the 1480 Wizard 3 gamma counter from Wallac (Turku, Finland). Results are expressed as %ID/g of tissue. Each value represents the mean and SD of two to five animals.

Blocking and Displacement Studies. Blocking and displacement studies were performed by injecting 3 mg/kg cyclo(-Arg-Gly-Asp-D-Phe-Val-) 10 min before or after injection of 370 kBq (10 μ Ci) of the radioactive compound (about 8 ng/mouse) in 100 μ L PBS pH 7.4. Animals were killed and dissected 60 min after injection of the 125 I-labeled peptides. Further processing was performed as described above.

Immunohistochemistry. Tumors were dissected and frozen using the deep freeze position of the cryomicrotome HM 500 O (-55°C ; Microm, Walldorf, Germany). Several 5 μm -thick sections were mounted on glass slides and immediately stored at -78°C . Histochemical staining was performed using hematoxylin and eosin (H&E).

For immunohistochemistry, frozen tissue sections were fixed in 4% (w/v) paraformaldehyde for 45 min and 0.1% (w/v) saponine for 30 min at room temperature and subsequently washed in Tris buffered saline and PBS. Human melanoma tissue sections were incubated with a monoclonal antibody directed against the human CD51/61 complex ($\alpha_v\beta_3$ integrin) (Boehringer Bioproducts, Heidelberg, Germany) at a final concentration of 2 $\mu\text{g}/\text{mL}$ in PBS, 2% (w/v) BSA for 1 h at room temperature. Tissue sections from murine osteosarcomas were incubated with a rabbit polyclonal antibody directed against the integrin α_v subunit (Boehringer Bioproducts) at an antisera dilution of 1:200. Tissues were washed extensively in PBS, and the secondary antimouse or antirabbit Alexa-488-labeled IgGs (Molecular Probes, Leiden, The Netherlands) were added at a working dilution of 1:1000 for 45 min at room temperature. Staining procedures in the absence of the primary antibodies and in the presence of control IgGs, respectively, served as controls. After five washes in PBS, slides were mounted and immunofluorescence was evaluated using a confocal laser scanning microscope (Zeiss, Göttingen, Germany).

Whole-Body Autoradiography. Osteosarcoma-bearing BALB/c mice received 100 kBq (2.7 μCi) [125 I]P2 per mouse intravenously, before being killed at 1 and 2 h, respectively (using ether anesthesia). The mice were frozen in an isopropanol-dry ice mixture, embedded in a 0.1% Methylan (Henkel, Germany) solution and frozen overnight at -20°C . Using a Leica CM 3600 Cryomicrotome (Nussloch, Germany), 40- μm sagittal plane sections were obtained, freeze-dried for 2 d and exposed for a period of 5 d. Images were developed using the phosphorimager from Molecular Dynamics (Krefeld, Germany).

RESULTS

In Vitro Binding Assay

The ability of cyclic pentapeptides to inhibit the binding of vitronectin and fibrinogen to the isolated immobilized $\alpha_{\text{Ib}}\beta_3$ and $\alpha_v\beta_3$ receptor was compared with the linear standard peptide Gly-Arg-Gly-Asp-Ser-Pro-Lys and with the lead structure cyclo(-Arg-Gly-Asp-D-Phe-Val-). The inhibitory peptides were able to suppress fully the binding of ligands to the isolated receptors, and the binding kinetics followed a classic sigmoid path. The inhibitory capacities (Table 2) of the modified peptides P1 to P4 are in the same range as the lead structure cyclo(-Arg-Gly-Asp-D-Phe-Val-), which shows IC_{50} values for the inhibition of the vitronectin

TABLE 2
Inhibition of Vitronectin Binding to Immobilized $\alpha_v\beta_3$ and Fibrinogen Binding to Immobilized $\alpha_{\text{Ib}}\beta_3$ (n = 3)

Number	Peptide	Q($\alpha_{\text{Ib}}\beta_3/\text{Fb}$)	Q($\alpha_v\beta_3/\text{Vn}$)
	GRGDSPK	1	1
	c(RGDfV)	1.9	0.033
P1	c(RGDyV)	2.5	0.030
P2	c(RGD(l)yV)	1.9	0.031
P3	c(RGDfY)	1.5	0.050
P4	c(RGDf(l)Y)	0.2	0.025
P5	c(RaDYV)	NA	NA

Fb = fibrinogen; Vn = vitronectin; NA = compound shows no activity in the test system.

To obtain intra-assay comparable results, we introduce normalized activities given as ratio $Q = \text{IC}_{50}[\text{peptide}]/\text{IC}_{50}[\text{GRGDSPK}]$.

binding to $\alpha_v\beta_3$ of 2 nmol/L and IC_{50} values for the inhibition of the fibrinogen binding to $\alpha_{\text{Ib}}\beta_3$ of 8000 nmol/L. The negative control peptide cyclo(-Arg-D-Ala-Asp-Tyr-Val-) P5 shows no activity in the range of the test system for both receptors. The selectivity of the peptides P1 to P4 corresponds with the selectivity of the lead structure. The biological activities are about 4000 times higher for the $\alpha_v\beta_3$ integrin than for the $\alpha_{\text{Ib}}\beta_3$ integrin.

Biodistribution Studies

For the biodistribution studies, three different tumor types were chosen: groups of nude mice bearing human melanoma M21 or mammary carcinoma (MaCaF), and BALB/c mice bearing osteosarcomas. The tissue distributions of the two peptides [125 I]P2 and [125 I]P4 are summarized in Tables 3 and 4, respectively.

Peptide [125 I]P2 showed an initial tumor uptake 10 min postinjection, with values ranging from 1.84 ± 0.17 %ID/g for the mammary carcinoma to 3.50 ± 0.49 %ID/g for the osteosarcoma. Sixty minutes postinjection, the highest tumor uptake was found for the osteosarcoma, followed by the melanoma M21 and the mammary carcinoma. The activities 60 min postinjection in the blood and the muscle reached values of 0.17 %ID/g and 0.25 %ID/g for the melanoma M21, 0.10 %ID/g and 0.16 %ID/g for the mammary carcinoma and 0.26 %ID/g and 0.43 %ID/g for the osteosarcoma (Fig. 3). This led to tumor-to-blood ratios 60 min postinjection of 7.7 for the melanoma M21, 7.4 for the mammary carcinoma and 7.8 for the osteosarcoma. The highest activity accumulations were found in the liver, with values >20 %ID/g 10 min postinjection to about 10 %ID/g 60 min postinjection, followed by the kidney.

Peptide [125 I]P4 was examined using BALB/c mice with osteosarcomas. Sixty minutes postinjection of [125 I]P4, most of the administered activity (about 75% ID/mouse) was detected in the intestine. All other examined organs showed only small amounts of the administered activity (Table 4). The tumor uptake was 0.40 ± 0.31 %ID/g 60 min postinjection. Even the activity accumulation in the liver (0.72 ± 0.14

TABLE 3
Activity Accumulation of [¹²⁵I]-3-iodo-D-Tyr⁴-cyclo(-Arg-Gly-Asp-D-Tyr-Val-) ([¹²⁵I]P2) in Nude Mice with Melanoma M21 (n = 3) or Mammary Carcinomas (n = 2) and BALB/c Mice with Osteosarcomas (n = 3)

	Melanoma M21			Osteosarcoma				Mammary carcinoma		
	10 min*	60 min	240 min	10 min*	60 min	120 min	240 min†	10 min	60 min	240 min
Blood	0.77 ± 0.02	0.17 ± 0.02	0.06 ± 0.02	1.72 ± 0.44	0.26 ± 0.03	0.17 ± 0.01	0.12 ± 0.02	0.73 ± 0.19	0.10 ± 0.01	0.09 ± 0.02
Plasma	1.43 ± 0.01	0.29 ± 0.03	0.09 ± 0.03	3.04 ± 0.82	0.43 ± 0.06	0.30 ± 0.02	0.21 ± 0.04	1.36 ± 0.30	0.17 ± 0.02	0.13 ± 0.04
Liver	21.96 ± 2.78	11.23 ± 1.95	0.78 ± 0.28	19.06 ± 0.92	10.36 ± 2.27	4.22 ± 1.91	2.18 ± 0.65	25‡	12‡	1.33 ± 1.05
Kidney	12‡	3.30 ± 0.12	0.72 ± 0.16	10.93 ± 2.37	2.64 ± 0.35	2.10 ± 0.23	1.08 ± 0.18	5.38 ± 0.66	1.05 ± 0.09	0.81 ± 0.53
Muscle	0.42 ± 0.04	0.25 ± 0.05	0.10 ± 0.03	0.94 ± 0.13	0.43 ± 0.05	0.36 ± 0.02	0.24 ± 0.04	0.48 ± 0.10	0.16 ± 0.02	0.14 ± 0.07
Thyroid	2.21 ± 0.64	3.45 ± 2.66	0.30 ± 0.08	3.49 ± 2.27	6.40 ± 2.27	15.61 ± 7.08	30.02 ± 11.2	5.40 ± 0.90	1.88 ± 0.16	4.90 ± 0.80
Tumor	2.07 ± 0.32	1.30 ± 0.13	0.41 ± 0.15	3.50 ± 0.49	2.03 ± 0.49	1.46 ± 0.16	0.92 ± 0.16	1.84 ± 0.17	0.74 ± 0.17	0.72‡
Tumor/ blood	2.7 ± 0.4	7.7 ± 1.2	6.8 ± 3.4	2.0 ± 0.6	7.8 ± 2.1	8.6 ± 1.1	7.7 ± 1.8	2.5 ± 0.7	7.4 ± 1.9	8.0 ± 1.8

*n = 2.

†n = 4.

‡Experiments gave only one data point.

Data given as %ID/g.

%ID/g 60 min postinjection) and kidney (0.78 ± 0.09 %ID/g 60 min postinjection) was low compared with [¹²⁵I]P2.

The tissue accumulation of the radiolabeled negative control peptide [¹²⁵I]P6 was investigated using nude mice with xenotransplanted melanoma M21 and BALB/c mice bearing osteosarcomas (Table 5, Fig. 4). The tumor uptake of [¹²⁵I]P6 10 min postinjection reached values of 1.12 ± 0.18 %ID/g for the melanoma M21 and 3.00 ± 0.71 %ID/g for the osteosarcoma. Thus, the initial uptake was about 45% lower for the melanoma and about 15% lower for the osteosarcoma, compared with [¹²⁵I]P2. In comparison with [¹²⁵I]P2, the tumor accumulation of [¹²⁵I]P6 in melanomas and osteosarcomas decreased much faster. The initial blood clearance of [¹²⁵I]P6 was slower than the clearance of [¹²⁵I]P2. However, for the melanoma M21-bearing nude mice, the [¹²⁵I]P6 accumulation in the blood reached the values of [¹²⁵I]P2 60 min after injection. For the osteosarcoma-bearing BALB/c mice, this accumulation remained 2- to 3-fold higher than for [¹²⁵I]P2. After 60 min postinjection, the activity concentrations of [¹²⁵I]P6 in the tumor reached the same low accumulation found in the blood (Fig. 4). The activity accumulation in the liver was in the same high range as that found for [¹²⁵I]P2, and the accumulation in the kidney was even higher than that found for [¹²⁵I]P2.

All radiolabeled peptides showed small activity accumulation in the thyroid. [¹²⁵I]P2 revealed the lowest iodine uptake

(values ranging between 0.3 %ID/g and 30 %ID/g), followed by [¹²⁵I]P6 (values between 4.4 %ID/g and 90 %ID/g) and [¹²⁵I]P4 (values about 75 %ID/g).

Pretreatment and Displacement Studies

The results of the pretreatment and displacement studies of [¹²⁵I]P2 are shown in Figure 5. Blocking with 3 mg/kg cyclo(-Arg-Gly-Asp-D-Phe-Val-) 10 min before the injection of [¹²⁵I]P2 reduced the tumor accumulation in the melanoma M21 model to about 40% of control and to about 35% of control in the osteosarcoma model. The displacement experiments with 3 mg/kg cyclo(-Arg-Gly-Asp-D-Phe-Val-) 10 min after injection of [¹²⁵I]P2 revealed similar trends: About 45% of the ¹²⁵I activity without cyclo(-Arg-Gly-Asp-D-Phe-Val-) was found in the melanomas as well as in the osteosarcomas. The same experiment with mammary carcinoma-bearing nude mice showed little effect. The tumor accumulation was reduced to only about 85% of the normal accumulation.

Immunohistochemistry

Immunohistochemistry performed on human melanoma (M21) tumor tissue sections from nude mice using the monoclonal antibody (LM609) directed against the human $\alpha_v\beta_3$ integrin revealed a positive and specific cell surface associated staining for $\alpha_v\beta_3$ (Fig. 6). Incubation of murine osteosarcoma tissue sections with a rabbit polyclonal antibody directed against the α_v integrin subunit also resulted in

TABLE 4
Activity Accumulation of [¹²⁵I]-3-iodo-Tyr⁶-cyclo(-Arg-Gly-Asp-D-Phe-Tyr-) ([¹²⁵I]P4) 60 Minutes Postinjection in BALB/c Mice with Osteosarcomas (n = 5)

Blood	Plasma	Liver	Kidney	Muscle	Thyroid	Intestine*	Tumor	Tumor/blood
0.35 ± 0.06	0.40 ± 0.08	0.72 ± 0.14	0.78 ± 0.09	0.15 ± 0.09	75 ± 78	45.1 ± 8.7	0.40 ± 0.10	1.1 ± 0.3

*n = 3.

Data given as %ID/g.

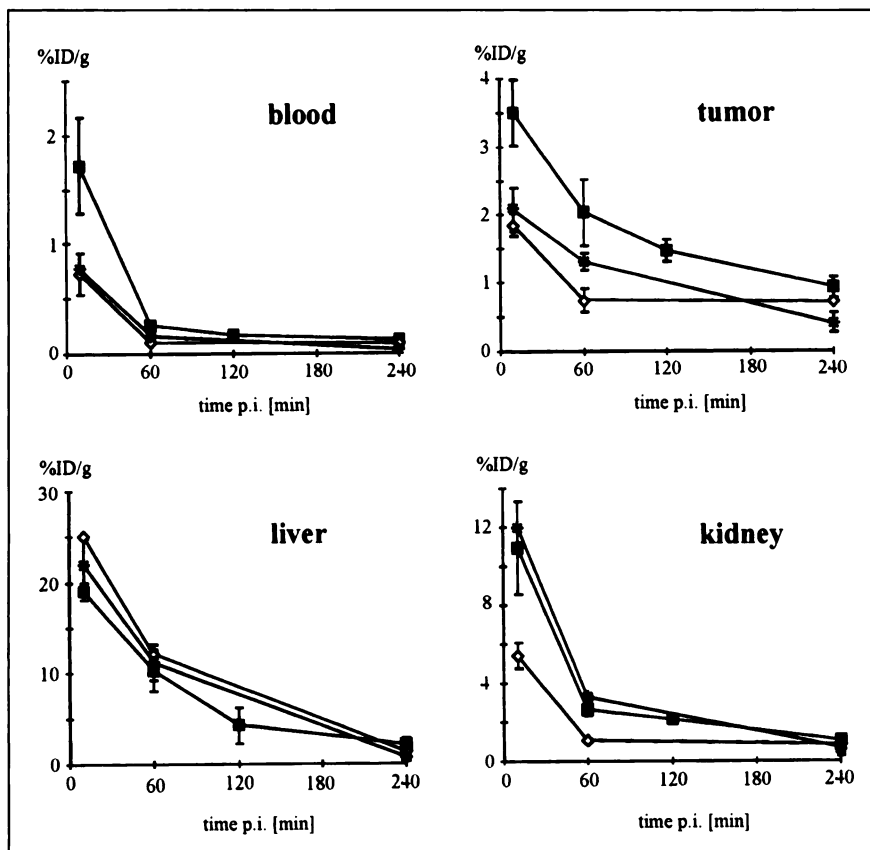


FIGURE 3. Biodistribution data of [¹²⁵I]-3-iodo-D-Tyr⁴-cyclo(-Arg-Gly-Asp-D-Tyr-Val-) ([¹²⁵I]P2) in nude mice bearing melanoma M21 (*) or mammary carcinoma (◇) and BALB/c mice with osteosarcoma (■).

a pronounced staining pattern for α_v . Incubation of tumor tissue with the respective control IgG showed only a weak and nonspecific staining.

Autoradiography

Whole-body autoradiographic imaging of BALB/c mice bearing osteosarcoma (Fig. 7) was performed 1 and 2 h after intravenous injection of 2.7 μ Ci [¹²⁵I]P2 per mouse. After 1 h, the highest activity accumulation was found in the liver and the spleen and, after 2 h, in the intestine. The accumulation in the tumor contrasted clearly with the background.

After 1 h, the accumulation was concentrated in the center of the tumor, where the ossified region was located and which was highly supplied with blood. After 2 h, the higher radioactivity accumulation was found in the cell-rich peripheral area of the tumor. As expected, there was no uptake in the brain.

DISCUSSION

The results of the isolated immobilized integrin receptor assay confirm our design approach. Substitution of D-Phe⁴ or

TABLE 5
Activity Accumulation of Negative Control Peptide [¹²⁵I]-3-iodo-Tyr⁴-cyclo(-Arg-D-Ala-Asp-Tyr-Val-) ([¹²⁵I]P6) in Nude Mice with Xenotransplanted Melanoma M21 (n = 4) and BALB/c Mice with Osteosarcomas (n = 3)

	Melanoma M21			Osteosarcoma		
	10 min	60 min	120 min	10 min	60 min	120 min
Blood	1.92 ± 0.34	0.24 ± 0.04	0.16 ± 0.06	4.46 ± 1.04	0.90 ± 0.92	0.48 ± 0.07
Plasma	3.20 ± 0.63	0.31 ± 0.08	0.19 ± 0.07	8.47 ± 2.36	1.93 ± 1.32	0.50 ± 0.06
Liver	24.5 ± 5.61	4.60 ± 1.34	0.78 ± 0.55	23.1 ± 7.19	12.56 ± 4.0	1.98 ± 0.44
Kidney	15.5 ± 2.69	4.42 ± 0.85	2.08 ± 0.80	26.5 ± 20.8	6.02 ± 2.18	1.55 ± 0.37
Muscle	0.48 ± 0.09	0.06 ± 0.03	0.03 ± 0.02	2.22 ± 2.33	0.31 ± 0.14	0.11 ± 0.04
Thyroid	6.52 ± 6.52	ND	10.1 ± 4.70	4.44 ± 1.37	42.8 ± 14.0	90.7 ± 13.5
Tumor	1.12 ± 0.18	0.31 ± 0.14	0.12 ± 0.04	3.00 ± 0.71	1.24 ± 0.37	0.48 ± 0.39
Tumor/blood	0.6 ± 0.1	1.3 ± 0.6	0.8 ± 0.4	0.7 ± 0.2	1.4 ± 1.5	1.0 ± 0.8

ND = not determined.
Data given as %ID/g.

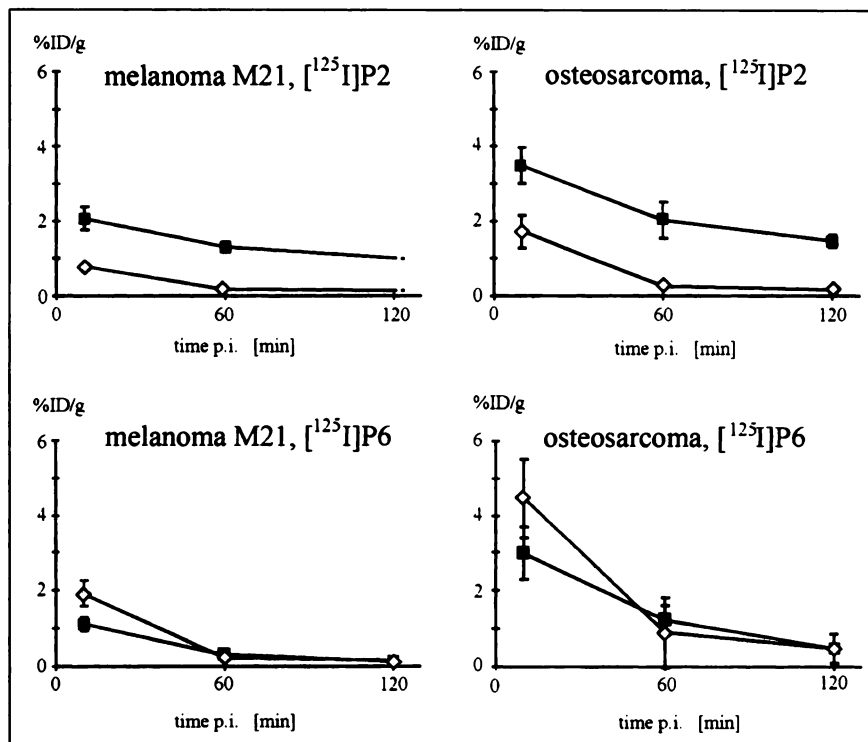


FIGURE 4. Activity accumulation of $\alpha_v\beta_3$ selective [^{125}I]-3-iodo-D-Tyr⁴-cyclo(-Arg-Gly-Asp-D-Tyr-Val-) ([^{125}I]P2) and negative control peptide [^{125}I]-3-iodo-D-Tyr⁴-cyclo(-Arg-D-Ala-Asp-Tyr-Val-) ([^{125}I]P6) in tumor (■) and blood (◇) of nude mice with xenotransplanted melanoma M21 and BALB/c mice bearing osteosarcomas.

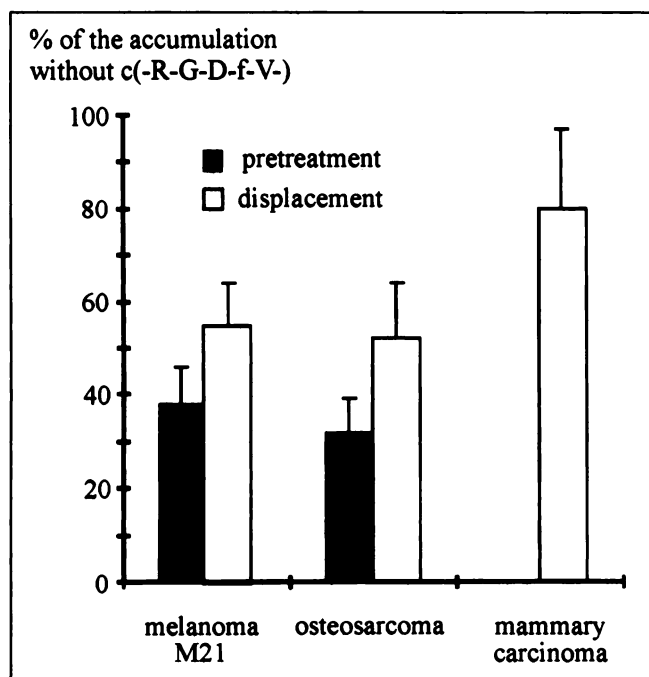


FIGURE 5. Pretreatment and displacement investigations using 3mg/kg $\alpha_v\beta_3$ selective cyclo(-Arg-Gly-Asp-D-Phe-Val-). Nude mice bearing melanoma and mammary carcinoma ($n = 3$) and BALB/c mice bearing osteosarcoma ($n = 3$) were used. Data were determined 60 min after injection of [^{125}I]P2. For pretreatment experiments, cyclo(-Arg-Gly-Asp-D-Phe-Val-) was injected 10 min before [^{125}I]P2 and for displacement experiments 10 min after [^{125}I]P2.

Val⁵ in the lead structure cyclo(-Arg-Gly-Asp-D-Phe-Val) with tyrosine and subsequent iodination of the modified peptides cyclo(-Arg-Gly-Asp-D-Tyr-Val-) P1 and cyclo(-Arg-Gly-Asp-D-Phe-Tyr-) P3 lead to compounds (P2, P4) with high affinity and selectivity for the $\alpha_v\beta_3$ integrin. In addition, the negative control peptide cyclo(-Arg-D-Ala-Asp-Tyr-Val-) P5, which is a modified version of the negative control cyclo(-Arg-D-Ala-Asp-Phe-Val-) (23), has no affinity for the two tested integrins. For P5, the iodinated cold reference compound was not tested, but we assume that, in analogy to the examined peptides P1 and P3, subsequent iodination has no significant influence on the binding affinity of P5.

The biodistribution studies show that the activity accumulation in the tumor 60 min postinjection is about 1.6 times higher for the osteosarcoma than for the melanoma M21 and about 2.7 times higher than for the mammary carcinoma. Pretreatment and displacement experiments suggest specific binding of [^{125}I]P2 to the melanoma M21 as well as to the osteosarcoma. It is known that the melanoma M21 cell line highly expresses the $\alpha_v\beta_3$ integrin (12,13). To prove $\alpha_v\beta_3$ expression on tumors grown in our animal models, immunohistochemistry has been performed (Fig. 6). Immunohistochemical staining in melanomas and osteosarcomas for $\alpha_v\beta_3$ and α_v , respectively, clearly indicates the presence of the $\alpha_v\beta_3$ integrin on the cell surface of both tumors in vivo. The whole-body autoradiographic images of the osteosarcoma-bearing BALB/c mice (Fig. 7) show that in the initial phase [^{125}I]P2 is accumulated in the ossified region of the tumor with high blood supply and later on is found in the areas of the osteosarcoma where the malign cell mass is concentrated. One explanation for this observation could be that in

the first phase the activity uptake is determined by the blood flow (highest accumulation in the regions with the best blood supply) and subsequently seems to depend on the $\alpha_v\beta_3$ integrin density (highest accumulation in the region of the malignant cells). The mammary carcinoma-bearing nude mice show only minor displacement. Therefore, the binding of [125 I]P2 to the mammary carcinoma seems to be nonspecific.

The specific behavior concerning the binding to the melanoma and the osteosarcoma is confirmed by investiga-

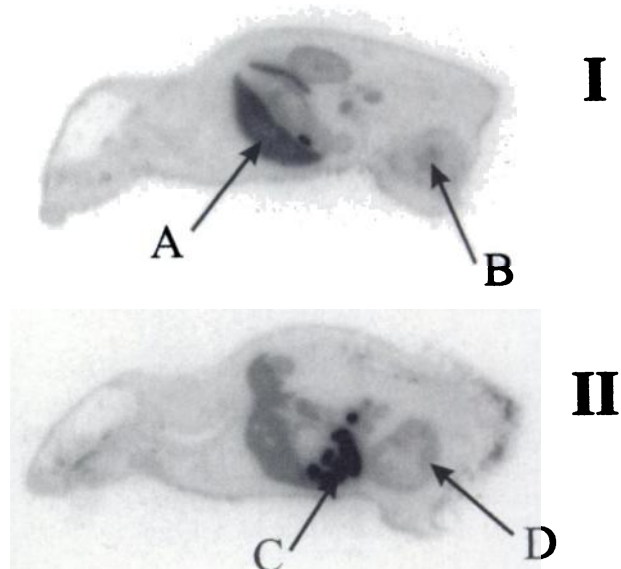
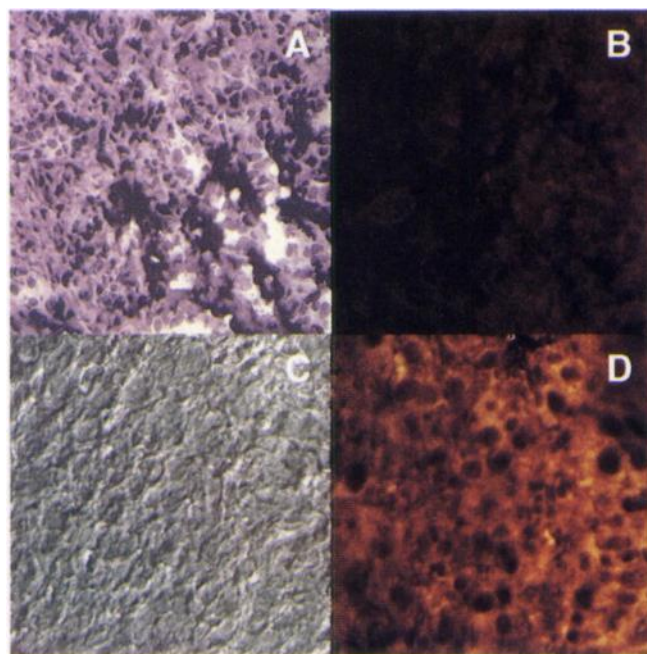
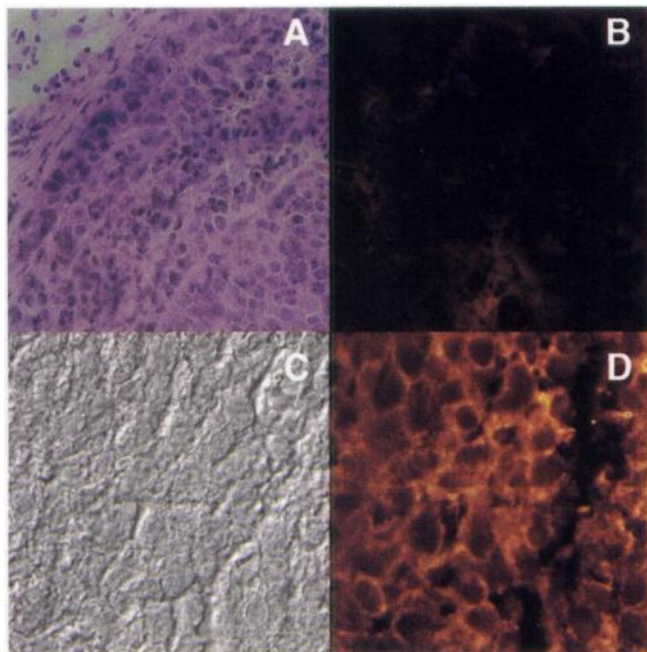


FIGURE 7. Whole-body autoradiographic images 60 min (I) and 120 min (II) after injection of [125 I]P2 confirm fast hepatobiliary elimination (liver [A], intestine [C]) and shows heterogeneous activity accumulation in osteosarcoma (B, D). After 60 min postinjection, activity is concentrated in center of tumor (B); after 120 min higher activity accumulation is found in peripheral area of tumor (D).

tions using the negative control peptide [125 I]P6. Figure 4 demonstrates that the activity concentration of [125 I]P6 in the tumor reveals the same low values as found in the blood 60 min postinjection and, thus, does not reflect specific $\alpha_v\beta_3$ binding, but rather blood flow. In contrast, the tissue accumulation of the $\alpha_v\beta_3$ selective [125 I]P2 for the osteosarcoma is between 2.0- and 8.6-fold and for the melanoma M21 is between 2.7- and 7.7-fold higher than the activity concentration in the blood for the whole observation time, indicating integrin-dependent accumulation of the tracer.

Another recently published approach (36–38), using phage-displaying RGD-containing peptides, revealed specific accumulation in the tumor tissue when injected intravenously into tumor-bearing mice. Immunohistochemical staining

FIGURE 6. Immunohistochemical detection of integrin $\alpha_v\beta_3$ in human melanoma and murine osteosarcoma tissue grown in vivo. Before performing immunohistochemistry, sections of each tumor type were stained with hematoxylin and eosin (H&E) (A) and presence of tumor material was classified as follows: Subcutaneous tissue of human melanoma M21 (top, A) revealed solid tumor mass with pleomorphic and hyperchromatic cells with mitosis. Murine osteosarcoma (bottom, A) exhibited pleomorphic tumor cells as well as areas with spindle-shaped cytoplasm, focal collagen fibers and production of osteoid matrix. Regions of melanoma and osteosarcoma positive tissue sections, classified with H&E staining (A), were stained with monoclonal antibody LM609 directed against $\alpha_v\beta_3$ and rabbit antibody directed against α_v , respectively (D). Respective transmission images are shown in C. Incubation of tumor tissue sections with control IgGs served as control stainings (B). Staining of tumor tissue (D) clearly demonstrates expression of $\alpha_v\beta_3$ integrins on both tumors.

showed that the RGD-containing phage bind to $\alpha_v\beta_3$ receptors present on endothelial cells of the tumor blood vessels and not to the tumor cells themselves (which are also $\alpha_v\beta_3$ positive). The reason for this effect is the large size of the phage, which makes it unlikely to exit the circulation and penetrate into tissues. However, these experiments confirm our approach using RGD-containing small peptides as tools in tumor targeting for diagnostic purposes (39,40). In addition, these peptides possess the advantage of diffusing efficiently within the tumor, which allows targeting of both kinds of $\alpha_v\beta_3$ positive cells.

The small activity accumulation in the thyroid gland for peptide [^{125}I]P2 (corresponding with about 0.01 %ID/g after 4 h postinjection) demonstrates remarkable in vivo stability toward deiodination. Even for [^{125}I]P6 with 90 %ID/g 120 min postinjection, this value corresponds to a low accumulation in the whole thyroid (0.2 %ID/g for a thyroid weight of 2 mg).

The data from the pharmacokinetic studies of [^{125}I]P2 and [^{125}I]P4 indicate fast blood clearance and predominantly hepatobiliary excretion, which, in the case of [^{125}I]P2, is also confirmed by whole-body autoradiographic imaging (Figs. 3 and 7). Because of this fast washout of peptides from the circulation, the activity accumulation in the tumor reaches an early maximum and continuously decreases. Therefore, improvement of the pharmacokinetics may lead to a higher activity accumulation in the tumor.

CONCLUSION

The radioiodinated $\alpha_v\beta_3$ antagonist [^{125}I]P2 exhibits high affinity for the $\alpha_v\beta_3$ integrin and specific binding to the melanoma M21 and to the osteosarcoma, with activity accumulations in the tumor of 1.30 ± 0.13 %ID/g 60 min postinjection and 2.03 ± 0.49 %ID/g 60 min postinjection, respectively. The biokinetics reveal predominantly hepatobiliary excretion and a fast blood clearance. Therefore, activity accumulation in the tumor reaches an early maximum (<10 min).

This study demonstrates that optimization of the new ligands concerning their biokinetic behavior is required before further investigations with other radioisotopes, such as ^{18}F or $^{99\text{m}}\text{Tc}$, are worthwhile. However, specific binding and tumor accumulation show that $\alpha_v\beta_3$ antagonists are a new group of promising tumor-imaging agents that may provide information about the $\alpha_v\beta_3$ receptor status of the tumor and should enable specific therapeutic planning. In addition, it may supply information on the metastatic potential of the tumor.

ACKNOWLEDGMENTS

This study was supported by grant 96.017.1 from the Sander-Stiftung and from the Pinguin-Stiftung. The authors thank Dr. Peter Heiss, Dr. Günther Reidel, Sabine Bernatz and Sabine Mayer (Department of Nuclear Medicine) for excellent technical assistance in carrying out the in vivo

experiments; Dr. Kurt Steiner (Merck KGaA) for providing the autoradiographic images; and Markus Urzinger (Institute of Organic Chemistry) for conducting the mass spectral analyses. Dr. Ingrid Becker (Pathology) is acknowledged for supplying the pictures of the histological sections. Parts of this study were presented at the 1997 annual meetings of the German Society of Nuclear Medicine and the Society of Nuclear Medicine.

REFERENCES

1. Reubi JC. Relevance of somatostatin receptors and other peptide receptors in pathology. *Endocr Pathol.* 1997;8:11–20.
2. Albelda SM. Biology of disease: role of integrins and other cell adhesion molecules in tumor progression and metastasis. *Lab Invest.* 1993;68:4–17.
3. Glukhova M, Deugnier MA, Thiery JP. Tumor progression: the role of cadherins and integrins. *Mol Med Today.* 1995;1:84–89.
4. Marshall JF, Hart IR. The role of α_v -integrins in tumour progression and metastasis. *Cancer Biol.* 1996;7:129–138.
5. Albelda SM, Buck CA. Integrins and other cell adhesion molecules. *FASEB J.* 1990;4:2868–2880.
6. Hynes RO. Integrins: versatility, modulation, and signaling in cell adhesion. *Cell.* 1992;69:11–25.
7. Ojima I, Chakravarty S, Dong Q. Antithrombotic agents: from RGD to peptide mimetics. *Bioorg Med Chem.* 1995;3:337–360.
8. Chorev M, Dresner-Pollak R, Eshel Y, Rosenblatt M. Approach to discovering novel therapeutic agents for osteoporosis based on integrin receptor blockade. *Biopolym. (Pep Sci.)* 1995;37:367–375.
9. Brooks PC, Clark RF, Cheresh DA. Requirement of vascular integrin $\alpha_v\beta_3$ for angiogenesis. *Science.* 1994;264:569–571.
10. Brooks PC, Montgomery AMP, Rosenfeld M, et al. Integrin $\alpha_v\beta_3$ antagonists promote tumor regression by inducing apoptosis of angiogenic blood vessels. *Cell.* 1994;79:1157–1164.
11. Brooks PC, Strömblad S, Klemke R, Visscher D, Sarkar FH, Cheresh DA. Antiintegrin $\alpha_v\beta_3$ blocks human breast cancer growth and angiogenesis in human skin. *J Clin Invest.* 1995;96:1815–1822.
12. Albelda SM, Mette SA, Elder DE, et al. Integrin distribution in malignant melanoma: association of the β_3 subunit with tumor progression. *Cancer Res.* 1990;50:6757–6764.
13. Felding-Habermann B, Mueller BM, Romerdahl CA, Cheresh DA. Involvement of α_v gene expression in human melanoma tumorigenicity. *J Clin Invest.* 1992;89:2018–2022.
14. Falcioni R, Cimino L, Gentileschi MP, et al. Expression of β_1 , β_3 , β_4 and β_5 integrins by human lung carcinoma cells of different histotypes. *Exp Cell Res.* 1994;210:113–122.
15. Lafrenie RM, Gallo S, Podor TJ, Buchanan MR, Orr FW. The relative roles of vitronectin receptor, E-selectin and $\alpha_4\beta_1$ in cancer cell adhesion to interleukin-1-treated endothelial cells. *Eur J Cancer.* 1994;30:2151–2158.
16. Gladson CL, Cheresh DA. Glioblastoma expression of vitronectin and the $\alpha_v\beta_3$ integrin. *J Clin Invest.* 1991;88:1924–1932.
17. Nip J, Shibata H, Loskutoff DJ, Cheresh DA, Brodt P. Human melanoma cells derived from lymphatic metastases use integrin $\alpha_v\beta_3$ to adhere to lymph node vitronectin. *J Clin Invest.* 1992;90:1406–1413.
18. Kawahara E, Ooi A, Nakanishi I. Integrin distribution in gastric carcinoma: association of β_3 and β_5 integrins with tumor invasiveness. *Pathol Int.* 1995;45:493–500.
19. Haubner R, Finsinger D, Kessler H. Stereoisomeric peptide libraries and peptidomimetics for designing selective inhibitors of the $\alpha_v\beta_3$ integrin for a new cancer therapy. *Angew Chem Int Ed Engl.* 1997;36:1374–1389.
20. Ruoslahti E, Pierschbacher MD. Arg-Gly-Asp: a versatile cell recognition signal. *Cell.* 1986;44:517–518.
21. Aumailley M, Gurrath M, Müller G, Calvete J, Timpl R, Kessler H. Arg-Gly-Asp constrained within cyclic pentapeptides: strong and selective inhibitors of cell adhesion to vitronectin and laminin fragment P1. *FEBS Lett.* 1991;291:50–54.
22. Gurrath M, Müller G, Kessler H, Aumailley M, Timpl R. Conformation/activity studies of rationally designed potent anti-adhesive RGD peptides. *Eur J Biochem.* 1992;210:911–921.
23. Pfaff M, Tangemann K, Müller B, et al. Selective recognition of cyclic RGD peptides of NMR defined conformation by $\alpha_{\text{IIb}}\beta_3$, $\alpha_v\beta_3$ and $\alpha_5\beta_1$ integrins. *J Biol Chem.* 1994;269:20233–20238.
24. Haubner R, Gratias R, Diefenbach B, Goodman SL, Jonczyk A, Kessler H. Structural and functional aspects of RGD-containing cyclic pentapeptides as

- highly potent and selective integrin $\alpha_v\beta_3$ antagonists. *J Am Chem Soc.* 1996;118:7461–7472.
25. Stöcklin G, Wester HJ. Strategies for radioligand development. Peptides for tumor targeting. In: Gulyas B, Müller-Gärtner HW, eds. *Positron Emission Tomography: A Critical Assessment of Recent Trends*. Dordrecht, The Netherlands: Kluwer Academic Publishers; 1998:57–90.
 26. Hom RK, Katzenellenbogen JA. Technetium-99m-labeled receptor-specific small-molecule radiopharmaceuticals: recent developments and encouraging results. *Nucl Med Biol.* 1997;24:485–498.
 27. König W, Geiger G. A new method for the synthesis of peptides: activation of the carboxyl group with dicyclohexylcarbodiimide using 1-hydroxybenzotriazoles as additives. *Chem Ber.* 1970;103:788–798.
 28. Chang CD, Waki M, Ahmad M, Meienhofer J, Lundell EO, Haug JD. Preparation and properties of N^ε-9-fluorenylmethyloxy-carbonyl amino acids bearing tert-butyl side chain protection. *Int J Pept Protein Res.* 1980;15:59–66.
 29. Yatohgo T, Kashiwagi H, Izumi M, Hayashi M. Novel purification of vitronectin from human plasma by heparin affinity chromatography. *Cell Struct Funct.* 1988;13:281–292.
 30. Kazal LA, Ansel S, Miller OP, Tocantins LM. The preparation and some properties of fibrinogen precipitated from human plasma by glycine. *Proc Soc Exp Biol Med.* 1963;113:989–994.
 31. Smith JW, Cheresch DA. The Arg-Gly-Asp binding domain of the vitronectin receptor photoaffinity cross-linking implicates amino acid residues 61–203 of the β -subunit. *J Biol Chem.* 1981;263:8726–8738.
 32. Mitjans FC, Sander D, Adán J, et al. An anti- α_v integrin antibody that blocks integrin function inhibiting the development of a human melanoma in nude mice. *J Cell Sci.* 1995;108:2825–2838.
 33. Cheresch DA, Spiro RC. Biosynthetic and functional properties of an Arg-Gly-Asp-directed receptor involved in human melanoma attachment to vitronectin, fibrinogen, and von Willebrand factor. *J Biol Chem.* 1987;262:7703–7711.
 34. Pytela R, Ginsberg MH, Pierschbacher MD, Plow EF, Ruoslahti E. Platelet membrane glycoprotein IIb/IIIa: member of a family of Arg-Gly-Asp specific adhesion receptors. *Science.* 1986;231:1559–1562.
 35. Senekowitsch R, Reidel G, Möllenstädt S, Kriegel H, Pabst HW. Curative radioimmunotherapy of human mammary carcinoma xenografts with iodine-131-labeled monoclonal antibodies. *J Nucl Med.* 1989;30:531–537.
 36. Pasqualini R, Koivunen E, Ruoslahti E. α_v integrins as receptors for tumor targeting by circulating ligands. *Nat Biotechnol.* 1997;15:542–546.
 37. Folkman J. Addressing tumor blood vessels. *Nat Biotechnol.* 1997;15:510.
 38. Arap W, Pasqualini R, Ruoslahti E. Cancer treatment by targeted drug delivery to tumor vasculature in a mouse model. *Science.* 1998;279:377–380.
 39. Haubner R, Wester HJ, Senekowitsch-Schmidtke R, et al. Radio-labeled RGD-peptides as tracer for tumor targeting and therapy control [in German] [abstract]. *Nuklearmedizin.* 1997;36:A93.
 40. Haubner R, Wester HJ, Senekowitsch-Schmidtke R, et al. Radiolabeled RGD-peptides: a new class of tracers for tumor targeting [abstract]. *J Nucl Med.* 1997;38:190P.